NEOPLASIA
www.neoplasia.com

Volume 20 Number 6 June 2018 pp. 594–609 **594**

Targeting Liver Cancer and Associated Pathologies in Mice with a Mitochondrial VDAC1-Based Peptide

Srinivas Pittala, Yakov Krelin and Varda Shoshan-Barmatz

Department of Life Sciences and the National Institute for Biotechnology in the Negev, Ben-Gurion University of the Negev, Beer-Sheva, 84105, Israel

Abstract

Hepatocellular carcinoma (HCC) is the third most lethal cancer worldwide. Despite progress in identifying risk factors, the incidence of HCC is increasing. Moreover, therapeutic options are limited and survival is poor. Therefore, alternative and innovative therapeutic strategies are urgently required. R-Tf-D-LP4, a cell-penetrating peptide derived from the mitochondrial multifunctional protein the voltage-dependent anion channel (VDAC1), is identified here as a highly effective liver cancer treatment. Recently, we demonstrated that R-Tf-D-LP4 induced apoptosis and inhibited tumor growth in mouse models. We now demonstrate that R-Tf-D-LP4 induced apoptosis in cancer liver-derived cell lines and inhibited tumor growth in three different liver cancer mouse models. These included diethylnitrosamine (DEN)-induced HCC, metabolically high-fat diet–induced HCC, and using a subcutaneous HepG2 cell xenograft model. Intravenous injection of the peptide into tumor-carrying DEN-treated mice resulted in dose-dependent inhibition of tumor growth up to complete tumor elimination. TUNEL staining of liver sections demonstrated peptide-induced apoptosis. Hematoxylin/eosin and Sirius red staining of liver sections showed decreased fibrotic formation. Immunohistochemical staining demonstrated reduced numbers of α-SMA–expressing cells in R-Tf-D-LP4–treated mouse livers. Additionally, macrophage presence in liver tissue was reduced in R-Tf-D-LP4–treated mice. Liver sections from DEN-treated mice showed steatohepatic pathology, reflected as fatty liver, inflammation, ballooning degeneration, and fibrosis; all were eliminated upon peptide treatment. Peptide treatment also inhibited tumor development in a nonalcoholic steatohepatitis–hepatocellular carcinoma mouse model induced by HFD. In HepG2 subcutaneous tumor xenografts, R-Tf-D-LP4 inhibited tumor growth. Conclusion: These results show that the VDAC1-based peptide R-Tf-D-LP4 has multiple effects on liver cancer cells, leading to impairment of cell energy and metabolism homeostasis, induction of apoptosis, and elimination of liver cancer-associated processes, and thus represents a promising therapeutic approach for liver cancer.

Neoplasia (2018) 20, 594–609

Introduction

Hepatocellular carcinoma (HCC) is a major form of adult primary liver cancer, the third most common cause of cancer-related deaths worldwide, and the second leading cause of death from malignancy following lung cancer [1]. The development of HCC has been associated with various risk factors, including viral infection, alcoholic-induced liver disease, nonalcoholic fatty liver disease and toxins, such as aflatoxin-B found in contaminated food [2]. Other risk factors for HCC include hereditary hemochromatosis, alpha-1-anti-trypsin deficiency, autoimmune hepatitis, and Wilson's disease [3].

Abbreviations: VDAC1, voltage-dependent anion channel 1; HK, hexokinase; Cyto *c*, cytochrome c; DEN, diethylnitrosamine; HCC, hepatocellular carcinoma; HFD, high fat diet; AIF, apoptosis-inducing factor; LDH, lactate dehydrogenase; NASH, nonalcoholic steatohepatitis; TfR, transferrin receptor.

Address all correspondence to: Varda Shoshan-Barmatz, Department of Life Sciences, Ben-Gurion University of the Negev, Beer-Sheva 84105, Israel.
E-mail: vardasb@bgu.ac.il

Received 8 November 2017; Revised 30 January 2018; Accepted 6 February 2018

1476-5586/17
https://doi.org/10.1016/j.neo.2018.02.012

Current therapeutic options are very limited, and survival after diagnosis is poor. Therefore, alternative and innovative therapeutic strategies are urgently required.

Mitochondria occupy a central position in cell life and death, playing crucial roles in cellular energy generation and metabolism, calcium homeostasis, cell signaling, proliferation, differentiation, and cell death, with mitochondria dysfunction having been implicated in many diseases, including cancer [4]. The voltage-dependent anion channel 1 (VDAC1) at the outer mitochondrial membrane serves as the mitochondrial gateway, mediating metabolic cross talk between the mitochondria and the rest of the cell [5–7]. VDAC1 is crucial for a range of cellular processes, including ATP rationing, Ca^{2+} homeostasis, apoptosis execution, and others [5,6,8,9]. These activities are regulated via the interaction of VDAC1 with many proteins central to the regulation of cell survival and cellular death pathways [4–6,8,9]. Thus, VDAC1, found at the crossroads of a variety of cell survival and cell death signals, serves as a controller of mitochondrial metabolism and apoptosis and thus can serve as a target for cancer therapy. VDAC1 is overexpressed in many other cancers [10,11], pointing to VDAC1 as playing a pivotal role in cancer cell survival [6,12].

Cancer cells utilize a variety of strategies to circumvent apoptosis, including quenching of the mitochondrial apoptotic pathway by overexpression of antiapoptotic proteins, such as Bcl-2 and hexokinase (HK-I, HK-II), thereby preventing the release of cytochrome *c* (Cyto *c*) from mitochondria [5,6,12–15]. VDAC1 functions in mitochondria-mediated apoptosis through its involvement in the release of apoptotic proteins to the cytosol and in the regulation of apoptosis via interaction with pro- and antiapoptotic proteins [16–21]. VDAC1 directly interacts with Bcl2 and Bcl-xL, leading to protection against apoptosis [19]. HK-I and HK-II interact with VDAC1 and, when overexpressed, prevented apoptosis in native but not mutated VDAC1-expressing cells [21–23]. Such proteins are highly expressed in many cancers and confer resistance to chemotherapy [24,25]. Thus, targeting cancer cell death evasion strategies by activating apoptosis and minimizing self-defense mechanisms of these cells are rational anticancer strategies. Accordingly, we engineered VDAC1-based peptides that interfere with the activity of the prosurvival proteins Bcl-2, Bcl-xl, and HK [16–21].

We have developed VDAC1-based peptides that effectively induced cancer cell death in a panel of genetically characterized cancer cell lines, regardless of cancer type or mutational status, with perceived specificity toward cancerous cells [16–21,26]. The peptides possess a triple mode of action, namely, energy and metabolism homeostasis impairment, interference with the action of antiapoptotic proteins, and triggering apoptosis [27]. VDAC1-based peptides represent new anticancer therapies, allowing for an overcoming of the chemoresistance of cancer cells.

Here, we used the VDAC1-based peptide R-Tf-D-LP4 to treat HCC. R-Tf-D-LP4 is a cell-penetrating peptide comprising a VDAC1-derived sequence termed LP4 containing amino acids in the D-conformation, fused to the human transferrin receptor (hTfR)-recognition sequence HAIYPRH (Tf). TfR is highly expressed in many different cancers, including liver cancers [28]. In three HCC mouse models, namely, chemically induced using diethylnitrosamine (DEN), metabolically induced using the high-fat diet (HFD)-32, and using subcutaneous Hep-G2 cell xenografts, the peptide dramatically reduced liver cancer. R-Tf-D-LP4 treatment of liver cancer is mediated via alteration of cancer cell metabolic activity, apoptosis induction, cell proliferation arrest, and reduced inflammatory and fibrotic activities. In addition, in a DEN-induced model, R-Tf-D-LP4–treated mice no longer showed steatohepatitis pathology. Thus, the R-Tf-D-LP4 peptide can serve as novel liver cancer therapy.

Materials and Methods

Materials

Carbonyl cyanide-p-trifluoromethoxyphenylhydrazone, DEN, leupeptine, phenylmethylsulfonyl fluoride, propidium iodide (PI), 4′,6-diamidino-2-phenylindole, trypan blue, glucose, beta-mercaptoethanol, dimethyl sulfoxide (DMSO), cytochalasin B, poly-(D, L-lactic-co-glycolide), and streptozotocin were purchased from Sigma (St. Louis, MO). Dithiothretol was purchased from Thermo Fisher Scientific (Waltham, MA). The cell transfection agent JetPRIME was from PolyPlus (Illkirch, France). Annexin-V was obtained from Alexis Biochemicals (Lausen, Switzerland). Dulbecco's modified Eagle's medium, 7.5% BSA solution, and the supplements fetal calf serum and penicillin-streptomycin were purchased from Biological Industries (Beit-Haemek, Israel). Tissue array sections (US Biomax) were purchased from (US Biomax Inc., Derwood, MD). Primary antibodies used in immunoblotting, immunohistochemistry (IHC) and immunoflouresence (IF), as well as their dilutions, are listed in Table 1. Horseradish peroxidase (HRP)–conjugated anti-mouse and anti-rabbit antibodies, TUNEL, and CellTiter-Glo Luminescent Cell Viability assay kits were obtained from Promega (Madison, WI). 3,3-Diaminobenzidine was obtained from (ImmPact-DAB, Burlingame, CA). The R-Tf-D-LP4 peptide (KWTWK-216-NSNGATWALNVATELKK-199-EWTWS**HRPYIAH)** was synthesized by GL Biochem (Shanghai, China) with >95% purity. The peptide was dissolved in DMSO and diluted to a stock solution of 5 mM in 5% DMSO, and its concentration was determined by following absorbance at 280 nm and using the specific molar extinction coefficient, as calculated based on amino acid composition (http://www.biomol.net/en/tools/proteinextinction.htm).

Cell Culture, R-Tf-D-LP4 Treatment, and Cell Death Analysis

Human HepG2, HuH7, and mouse BNL1MEA.7R.1 liver cancer cell lines were maintained at 37°C in a 5% CO_2 atmosphere in the recommended culture medium and supplements added with 10% fetal calf serum, 1 mM L-glutamine, 100 U/ml penicillin, and 100 μg/ml streptomycin.

For peptide treatment, cells ($1.5\text{-}2 \times 10^5$ cells/well) were incubated for 6 hours in serum-free medium with various concentrations of the peptide at 37°C. Cell death was analyzed by PI and Annexin V-FITC staining by flow cytometery.

Mitochondria-Bound HK Detachment and Cytochrome C Release Assays

Peptide-induced HK detachment from mitochondria to the cytosol was assessed using HepG2 cells expressing GFP-HK-I. HK-I/II mitochondrial detachment and Cyto *c* release to the cytosol were analyzed by subcellular fractionation into cytosolic and mitochondria fractions and immunoblotting using anti-HK-I or anti–Cyto *c* antibodies. Images were captured using a confocal microscope (Olympus 1X81).

HepG2 cells (3×10^5) were incubated for 3 hours with R-Tf-D-LP4 (3, 5, 10 μM). The cells were harvested, washed with PBS, and gently resuspended in ice-cold buffer (100 mM KCl, 2.5 mM $MgCl_2$, 250 mM sucrose, 20 mM HEPES/KOH, pH 7.5, 0.2 mM EDTA, 1 μg/ml leupeptin, 5 μg/ml cytochalasin B, and 0.1 mM phenylmethylsulfonyl fluoride) containing 0.02% digitonin and incubated for 10 minutes on ice. Aliquots were centrifuged at

Table 1. Antibodies used in this study.

Antibody	Source and Catalog No.	Dilution		
		IHC	WB	IF
Mouse monoclonal anti-actin	Millipore, Billerica, MA, MAB1501	-	1:40000	-
Rabbit polyclonal anti-AIF	Abcam, Cambridge, UK, ab32516	1:200	1:1000	-
Rabbit polyclonal anti-alpha smooth muscle actin antibody	Abcam, Cambridge, UK, ab5694	1:200	-	-
Mouse monoclonal anti-ATP5a	Abcam, Cambridge, UK, ab14748	1:300	-	-
Rat monoclonal anti-CD45R (B220)	Ebioscience, CA, USA, 11-0452-82	-	-	1:300
Rabbit polyclonal anti-Bcl-xL	Abcam, Cambridge, UK, ab32516	-	1:2000	-
Rabbit polyclonal anti-caspase 3	Cell Signaling Technology, Danvers, MA, 9662	-	1:2000	-
Rabbit monoclonal anti-caspase 8	Abcam, Cambridge, UK, ab108333	-	1:1000	-
Armenian hamster monoclonal-CD3e (145-2C11), FITC	Ebioscience, CA, USA, 36-0031-85	-	-	1:300
Rabbit polyclonal anti-CD4	Abnova, Taiwan, PAB19557	-	-	1:300
Mouse monoclonal anti-CD8	Biolegend, San Diego, CA, 100702	-	-	1:300
Rabbit polyclonal anti-citrate synthase	Abcam, Cambridge, UK ab96600	1:200	-	-
Mouse monoclonal anti-cytochrome *c*	BD Bioscience, San Jose, CA, 556432	1:300	1:2000	-
Rat monoclonal anti-F4/80	Santa Cruz Biotechnology, Inc. Dallas, TX, sc52664	1:150	-	-
Mouse monoclonal anti-FOXP3	Biolegend, San Diego, CA, 126402	-	-	1:300
Mouse monoclonal anti-GAPDH	Abcam, Cambridge, UK, ab9484	1: 200	-	-
Rabbit monoclonal anti-Glut1	Abcam, Cambridge, UK ab40084	1: 200		-
Mouse monoclonal anti-HK-I	Abcam, Cambridge, UK ab105213	-	1:2000	-
Rabbit polyclonal anti-HK II	Abcam, Cambridge, UK ab3279	1:400	1:2000	-
Rabbit monoclonal anti-Ki67	Thermo Scientific, NY RM-9106-s1	1:200	-	-
Goat polyclonal anti-LDH-A	Santa Cruz Biotechnology, Inc. Dallas, TX,sc-27230	1:200	-	-
Rabbit polyclonal anti-TfR	Abcam, Cambridge, UK, ab84036	-	1:2000	-
Rabbit monoclonal anti-VDAC1	Abcam, Cambridge, UK,ab15895	1:500	1:5000	-
Donkey anti-Goat-HRP	Abcam, Cambridge, UK, ab97120	1:500	-	-
Goat anti-Mouse-HRP	Abcam, Cambridge, UK, ab97040	1:250	1:10,000	
Donkey anti-Mouse (Alexa Fluor 488)	Abcam, Cambridge, UK, ab150109	-	-	1:1000
Goat anti-Rabbit-HRP	KPL, Gaithersburg, USA, 474-1506	1:500	1:15,000	-
Goat anti-Rabbit (FITC)	Ebioscience, CA, USA, 65-6111	-	-	1:500
Goat anti-Rat-HRP	Santa Cruz Biotechnology, Inc. Dallas, TX, sc-2006	1:500	-	-

Antibodies against the indicated protein, their catalogue number, source and the dilutions used in IHC and immunoblot experiments were presented.

12,000×*g* at 4°C for 10 minutes to obtain the cytosolic fraction, from which aliquots were subjected to SDS-PAGE and immunoprobed with anti–HK-I (1:2000) or anti–Cyto *c* antibodies (1:2000).

Determination of Cellular ATP Levels

Cellular ATP levels were estimated using a luciferase-based assay (CellTiter-Glo, Promega). HepG2 cells (3×10^5 cells/ml) were incubated with the indicated concentrations of R-Tf-D-LP4 peptide for 3 hours, washed twice with PBS, and transferred to 96-well white plates (1×10^5 cells/100 µl/ well). ATP levels were assayed according to the manufacturer's protocol, and luminescence was recorded using an Infinite M1000 plate reader (Tecan, Männedorf, Switzerland).

High-Fat Diet-32 (HFD-32) Food Composition

HFD-32 food was prepared as described previously [29] and comprised (w/w) 5% egg white powder (MM Ingredients, Wimborne, UK); 6.928% lactose (Sigma); 15.88% beef fat (saturated) powder (containing 80% beef fat) (MP Biomedical, Illkirch, France); 24.5% milk casein (Shaanxi Fuheng Biotechnology, Xi'an, China); 20% safflower oil (high oleic acid type) (Bustan a Briut, Galil, Israel); 6.45% sucrose (Sigma); 0.36% choline bitartrate (Bulk Powders, Colchester, UK); 5.5% crystalline cellulose (Sigma); 0.43% L-cysteine (Source Naturals, Scotts Valley, Santa Cruz, CA); 8.25% maltodextrin (Bulk Powders); 5% AIN93G-mineral mixture (MP Biomedical); 1.4% AIN93VX-vitamin mix (MP Biomedical); and 0.002% tertiary butyl hydroquinone (MP Biomedical). C57Bl/6 control mice were fed a standard chow diet.

HCC mouse models

(a) DEN-induced liver cancer was induced as described previously [30]. Briefly, 2-week-old male C57BL/6 mice received intraperitoneal injections of DEN (20 mg/kg), and about 30 weeks later, tumors developed in the liver. Tumor development was confirmed by sacrificing several mice or using MRI. Peptide treatment began on week 32 by intravenous (i.v.) tail vein injection of HBSS (5.33 mM KCl, 0.44 mM KH_2PO_4, 138 mM NaCl, 4 mM $NaHCO_3$, 0.3 mM Na_2HPO4, and 5.6 mM glucose, pH 7.3) or R-Tf-D-LP4 (10, 14, n = 10 or 18 mg/kg, 30 mice/group) three times a week up to week 43. The final concentration of DMSO in the blood was calculated as 0.07% in both groups.

At week 42, the mice were visualized by MRI. At week 43, the mice were sacrificed, and their livers were excised and weighed. Half of each liver was either fixed in 4% buffered formaldehyde, paraffin embedded, and processed for IHC or frozen in liquid nitrogen for later immunoblotting.

(b) HFD-32–induced HCC, known as the STAM mouse model, was produced as described previously [29]. Briefly, 2-day-old C57BL/6 male pups were injected subcutaneously (s.c.) with streptozotocin (STZ) (200 µg/mouse) and fed an HFD-32 diet from the age of 4 weeks. HFD-32–fed mice developed hepatocellular carcinomas by week 16 to 18. Treatment with HBSS or R-Tf-D-LP4 (14 mg/kg) (final DMSO blood concentration was 0.07% in both groups) took place three times a week from weeks 16 to 22, when the mice were sacrificed and their livers were excised and *ex vivo* weighed. Each liver was fixed in 4% buffered formaldehyde, paraffin embedded, and processed for hematoxylin-eosin (H&E) staining.

(c) Xenograft mouse model in which HepG2 cells (2×10^6) were inoculated by s.c. injection into the hind leg flanks of athymic nude 8-week-old male nude mice (Envigo, Israel). Eleven days

post–cell inoculation, tumors were measured using a digital caliper, and volumes were calculated using the formula: $r_1^2 \times r_2/2$ (r_1 is the shortest and r_2 is the longest diameter). When tumor volume reached 75 to 100 mm^3, the mice were randomly divided into two groups (5 mice/group). One group was intratumorally injected with HBSS containing 0.04% DMSO and the second group with the peptide in HBSS containing 0.05% DMSO, with the peptide at a final concentration of 40 to 60 μM. The xenografts were injected 20 μl per tumor (2 points) every 2 days. Mouse weight and tumor volumes were monitored twice a week. At the end of the experiments, the mice were sacrificed, and tumors were excised, photographed, and *ex vivo* weighed. Half of each tumor was fixed in 4% buffered formaldehyde, paraffin embedded and processed for IHC, while the second half was frozen in liquid nitrogen for immunoblotting analysis.

The experimental protocols followed were approved by the Institutional Animal Care and Use Committee of Ben-Gurion University.

MRI Tumor Monitoring

In vivo mouse body MRI was performed using the M7 1-T compact ICON system (Aspect Imaging, M7, Israel), equipped with a set of 80 mm application-specific radiofrequency (RF) mouse body coil. For *in vivo* imaging, animals were maintained in an anesthetized state with 1.5% isoflurane in O_2 and placed on a specially designed heated bed where physiological signals, such as breath rate, were monitored throughout the experiment to ensure animal well-being. MRI acquisition parameters included fast spin echo with a repetition time of 3440 milliseconds and an echo time of 83 milliseconds. Fifteen coronal slices of 1.2 mm with a gap of 1.4 mm and a matrix of 268 × 120, a field of view of 40 × 80 mm, and an acquisition time of 14.35 minutes were collected.

Gel Electrophoresis and Immunoblotting

Cells or tumor tissue were lysed using lysis buffer (50 mM Tris-HCl, pH 7.5, 150 mM NaCl, 1 mM EDTA, 1.5 mM $MgCl_2$, 10% glycerol, 1% Triton X-100) supplemented with a protease inhibitor cocktail (Calbiochem, Billerica, MA). Cell lysates were then centrifuged at 600×*g* (10 minute at 4°C), and samples (10-40 μg of protein) were subjected to SDS-PAGE and immunoblotting using various primary antibodies (sources and dilutions as detailed in Table 1), followed by the appropriate HRP-conjugated secondary antibodies (1:20,000). Blots were developed using enhanced chemiluminescence (Biological Industries). Band intensities were analyzed by densitometry using Fusion FX software (Vilber), and the values were normalized to the intensities of the appropriate β-actin signal that served as a loading control.

IHC and Immunofluorescent (IF) Staining of Tissue Sections

Formalin-fixed, paraffin-embedded sections of livers from the different experiments were H&E stained and probed with appropriate antibodies for IHC or IF staining. IHC or IF staining was performed on 5-μm-thick formalin-fixed and paraffin-embedded liver or tumor sections. The sections were deparaffinized by placing the slides on a heating plate set at 60°C for 1 hour and using xylene. Thereafter, the tissue sections were rehydrated with a graded ethanol series (100% to 50%). Antigen retrieval for some proteins [ATP synthase 5a, apoptosis inducing factor (AIF), citrate synthase, Cyto c, glyceraldehyde dehydrogenase (GAPDH), HK-II, VDAC1, CD3, B220 and Glut1] was performed in 0.01 M citrate buffer (pH 6.0). For HK-I, lactate dehydrogenase A (LDHA), Ki-67, F4/80, CD4, CD8, FOXP3, and α-SMA, antigen retrieval was performed in 10 mM Tris-EDTA (pH 9) and 0.5 M Tris-EDTA (pH 10) for 30 minutes each at 95°C to 98°C. After washing sections in PBS containing 0.1% Triton-X100 (pH 7.4), nonspecific antibody binding was reduced by incubating the sections in 10% normal goat serum for 2 hours. After decanting excess serum, the sections were incubated overnight at 4°C with primary antibodies (sources and dilutions used detailed in Table 1) and washed with PBST. For IHC, endogenous peroxidase activity was blocked by incubating the sections in 3% H_2O_2 for 15 minutes. After washing thoroughly with PBST, the sections were incubated with the appropriate secondary antibodies for 2 hours. For IHC, anti-mouse, anti-goat, or anti-rabbit secondary antibodies conjugated to HRP were used. Sections were washed five times in PBST (PBS, 0.1% Tween-20), and the peroxidase reaction was subsequently visualized by incubating with 3,3-diaminobenzidine. After rinsing in water, the sections were counterstained with hematoxylin and mounted with Eukitt mounting medium. Finally, the sections were observed under a microscope (Leica DM2500), and images were collected at 20× magnification with the same light intensity and exposure time. Nonspecific control experiments were carried out using the same protocols but omitting incubation with the primary antibodies. H&E staining was performed as described previously [31]. The stained sections were scanned with a panoramic scanner (panoramic MIDI II, 3DHISTH). Quantification of the immunostained images generated was carried out using HistoQuant software (Quant Center 2.0 software, 3DHISTH). For IF, images were captured using a confocal microscope (Olympus 1X81).

Sirius Red Collagen Staining

Sirius red staining of paraffin-embedded sections was carried out using an established methodology [32]. Briefly, sections of liver tissue fixed and embedded in paraffin were stained with a 0.1% Sirius red–1.3% picric acid solution. Sections were washed rapidly with acetic acid (0.5%), and images were obtained using a microscope (Leica DM2500).

TUNEL Assay

Paraffin-embedded fixed tumors sections were processed for a TUNEL assay using the DeadEnd Fluorometric TUNEL system (Promega, Madison, WI) according to the manufacturer's instructions. Sections were deparaffinized, equilibrated in PBS, permeabilized with proteinase K, postfixed in 4% paraformaldehyde, and incubated in TdT reaction mix for 1 hour at 37°C in the dark. Sections were then washed with 2× SSC buffer (0.3 M NaCl, 30 mM trisodium citrate, pH 7.0), counterstained with PI (1 μg/ml), and coverslipped with Vectashield mounting medium. Fluorescent images of apoptotic cells (green) and cell nuclei (red) were captured using a confocal microscope (Olympus 1X81).

Statistics and Data Analysis

Means ± SE of results obtained from three to five independent experiments are presented. A nonparametric Mann-Whitney *U* test was used to compare control and experimental groups. A difference was considered statistically significant when the *P* value was deemed <.05 (*), <.01 (**), <.001 (***), or <.0001 (****).

Results

In this study, we assessed the effects of a cell-penetrating VDAC1-based peptide, R-Tf-D-LP4, both *in vitro* in liver cancer-derived cell lines and *in vivo* in three characterized liver cancer mouse models, namely,

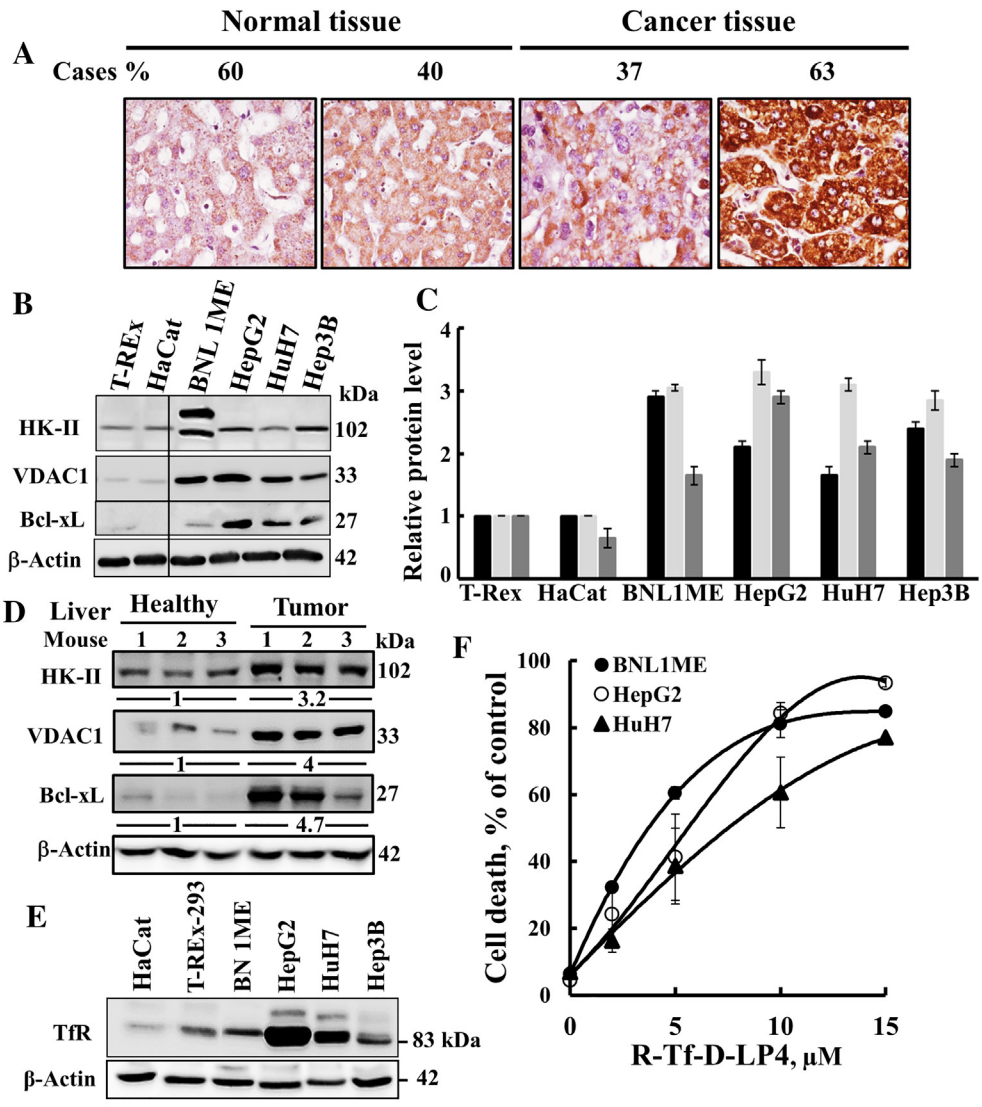

G

Cell line	Origin	Mutations	R-Tf-D-LP4 IC_{50} μM
HepG2	Human hepato-cellular carcinoma	CTNNB1, NRAS	3.76 ± 0.86
HuH7	Human hepato-cellular carcinoma	TP53, FOXP1, ABI1, AMER1, ALK, CYLD, MAX, ROS1, FANCD2	5.35 ± 0.85
BNL 1ME A.7R.1	Mouse-embryo liver chemically transformed	Not reported	7.6 ± 0.17

Figure 1. VDAC1 is overexpressed in liver tumor and cancer cell lines, and cell death is inducted by the VDAC1-based peptide R-Tf-D-LP4. (A) Tissue array (US Biomax) comprising human normal liver (n = 5) and liver cancer (n = 19) sections stained with anti-VDAC1 antibodies. Percentages of sections stained at the intensity indicated are shown. Immunoblot analysis of HK-II, VDAC1, and Bcl-xL (B) expression in noncancerous and liver cancer-derived cells. (C). The levels of HK-II (black bars), VDAC1 (light grey bars), and Bcl-xL (dark bars) in the indicated cell line are presented relative to their expression levels in the T-REx-293 cell line. (D) Immunoblot analysis of HK-II, VDAC1, and Bcl-xL expression in livers from healthy and DEN-treated mouse cancer-derived livers (n = 3). The fold increase in protein expression levels is also indicated. (E) Immunoblotting of TfR expression in noncancerous and liver cancer-derived cell lines. (F) R-Tf-D-LP4 effectively induced cell death of liver tumor cell lines. Human HepG2 (○), HuH7 (▲), and mouse BNL1MEA.7R.1 cells (●) were incubated for 6 hours with R-Tf-D-LP4, and cell death was analyzed as described in Materials and Methods. (G) IC_{50} values (μM) for peptide-induced apoptosis in liver tumor cell lines with the various indicated mutations [49]. Results show means ± SD (n = 3).

chemically DEN induced, metabolically (HFD-32 STAM model) induced HCC, and using subcutaneous HepG2 cell xenografts.

VDAC1 is overexpressed in a variety cancer types [10,11]. The expression levels of VDAC1 in liver cancer were assessed by IHC of a tissue microarray containing 20 patient-derived liver cancer samples and healthy liver-derived sections using VDAC1-specific antibodies. Liver tumor samples showed a marked increase in VDAC1 expression levels relative to the healthy liver sections (Figure 1*A*). Similarly, immunoblotting demonstrated that VDAC1 expression levels in cancerous cell lines, including human HuH7, HepG2, and mouse BNL1MEA.7R.1 cells, were some three-fold higher than in the noncancerous immortalized TREx-293 and HaCaT cell lines (Figure 1, *B* and *C*).

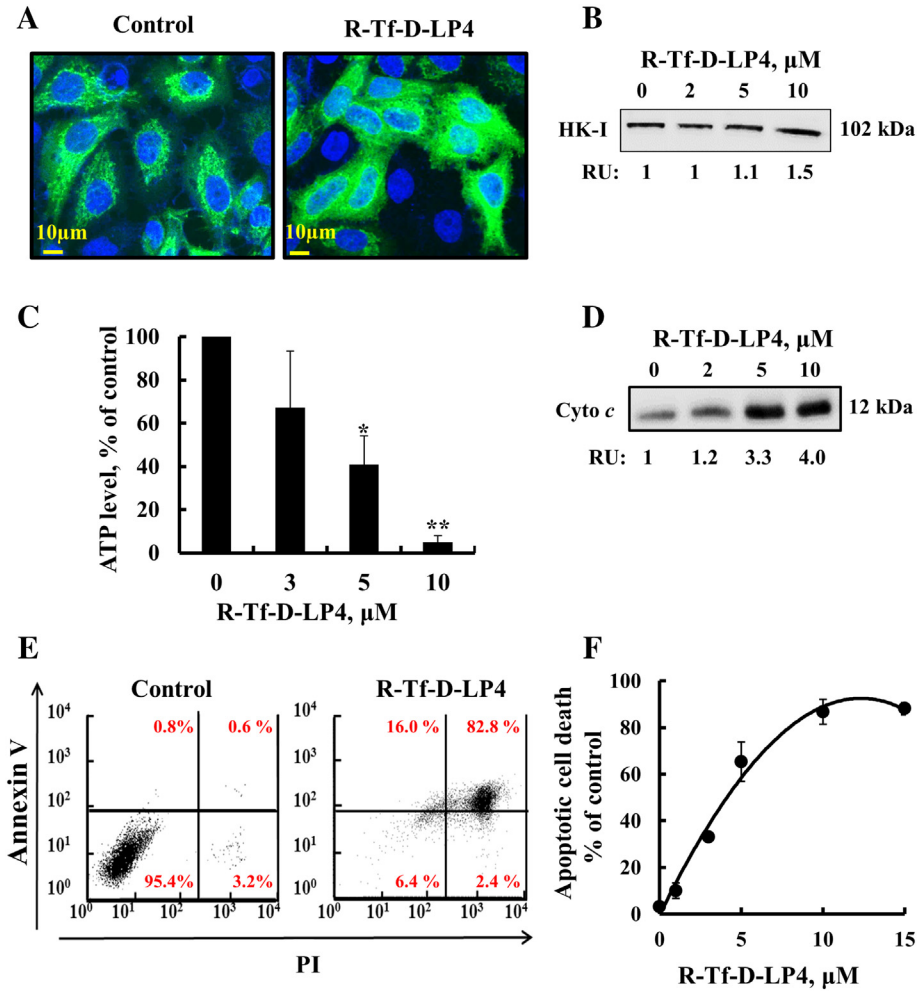

Figure 2. R-Tf-D-LP4 induces cell death: mode of action.R-Tf-D-LP4 induces detachment of HK-I-GFP (A) and endogenous HK-I in HepG2 cells analyzed by immunoblotting of cytosolic fraction and presented as relative units (B), as described in Materials and Methods. (C) R-Tf-D-LP4 reduces cellular ATP levels, assayed as described in Materials and Methods. Results show means ±SE ($n = 3$) (*$P \leq .05$, **$P \leq .01$). (D) R-Tf-D-LP4–induced Cyto *c* release from mitochondria was analyzed by immunoblotting cytosolic fraction as described in Materials and Methods. (E, F) R-Tf-D-LP4–induced apoptosis as analyzed by Annexin V-FITC and PI staining and flow cytometry. Representative FACS analysis of control and R-Tf-D-LP4 (5 µM)–treated HepG2 cells (E). Apoptosis as a function of R-Tf-D-LP4 concentration. Results show means ±SE ($n = 3$).

The overexpression of VDAC1 points to its important metabolic function in liver cancer cell growth and tumor development [10,33,34].

VDAC1 overexpression has been shown to induce apoptotic cell death [5,6], although cancer cells overexpressing VDAC1 survive. This is most likely due to overexpression of VDAC1-interacting antiapoptotic proteins, such as HK, Bcl-2, and Bcl-XL [5,6,12–15]. Indeed, the levels of the glycolytic enzyme HK-II and of the antiapoptotic protein Bcl-xL were higher in the cancerous liver cell lines than in the noncancerous cell lines (Figure 1*B*). Quantitative analysis of the expression levels of these proteins in the cancer cell lines, relative to their expression in the noncancerous TRE-x-293 cell line, revealed a 1.5- to 3.5-fold increase (Figure 1*C*). Moreover, VDAC1, HK-II, and Bcl-XL were highly overexpressed (three- to five-fold) in liver containing tumors (DEN model, see below) relative to healthy mouse livers (D).

The VDAC1-Based Peptide Induces Apoptotic Cell Death

In our previous studies [26,35], we designed and tested over 40 versions of VDAC1-based cell-penetrating peptides. Of these, we selected the cell-penetrating R-Tf-D-LP4 peptide comprising a VDAC1-derived sequence, defined as LP4, fused to a hTfR-recognition sequence HAIYPRH (Tf) [28], with the peptide amino acids sequence, except of Tf, being in D-configuration, making it more resistant to proteolytic degradation. The peptide also presents a reverse sequence, allowing it to maintain side chain topology similar to that of the original L-amino acid peptide. hTfR is highly expressed in many cancers [28], including HCC [36], allowing targeting of the peptide to cancer cells. Indeed, HCC cell lines of mouse and human origin, such as human HuH7 and HepG2 and mouse BNL1MEA.7R.1 cells, showed high expression of TfR relative to noncancerous cells, such as HaCat and T-REx-293 cells (Figure 1*E*).

Incubation of the HepG2, HuH7, and BNL1MEA.7R1 cell lines with R-Tf-D-LP4 resulted in marked cell death (Figure 1*F*). In the HCC-derived cell lines tested, regardless of mutational status, similar peptide concentrations (3.8 to 7.6 µM) were required for realizing half-maximal (IC_{50}) activity (Figure 1*G*).

The mode of action of R-Tf-D-LP4 was studied by assessing the detachment of mitochondria-bound HK, decrease in cellular ATP levels, and induction of Cyto *c* release and apoptosis (Figure 2). As VDAC1-based peptides interact with HK [20,21,37,38], HK-I

detachment from VDAC1 was analyzed using two approaches, namely, expression of HK-I-GFP and testing the effect of R-Tf-D-LP4 on HK-I-GFP cellular distribution (Figure 2*A*) or by subcellular fractionation into cytosolic and mitochondrial fractions and looking for HK-1 by immunoblot (Figure 2*B*). Confocal fluorescence microscopy showed that, in control cells, HK-I-GFP fluorescence was punctuated, as expected for mitochondrial distribution. However, HK-I-GFP fluorescence in R-Tf-D-LP4–treated cells was diffuse, indicating cytosolic distribution (Figure 2*A* (This was further supported by the presence of HK-I in the cytosolic fraction of the peptide-treated cells (Figure 2*B*).

R-Tf-D-LP4–treated cells showed decreased cellular ATP levels (90%) (Figure 2*C*). These results suggest that the peptide-induced decrease in energy production was due to HK detachment from VDAC1. By detaching HK that catalyzes the first step of glycolysis, glycolysis is inhibited. Consequently, TCA cycle activity is decreased as less acetyl-CoA is produced from pyruvate. This leads to an uncoupling of glycolysis from oxidative phosphorylation [39]. The decrease in ATP levels also resulted from respiratory inhibition upon Cyto *c* release from the mitochondria. The effect of the peptide on Cyto *c* release was analyzed in HepG2 cells by cell fractionation and immunoblotting using anti–Cyto *c* antibodies. Cyto *c* levels were highly increased in the cytosolic fraction from peptide-treated cells (Figure 2*D*). Finally, R-Tf-D-LP4–treated HepG2 cells showed over 90% cell death, as revealed by Annexin V/PI staining and cell sorting analysis, with an IC_{50} of 4.5 μM (Figure 2, *E* and *F*).

Thus, in HCC cells, the mode of action of R-Tf-D-LP4 is similar to its mode of action in other cancer cell lines [26,35].

R-Tf-D-LP4–Mediated Treatment of DEN-Induced HCC

DEN, a chemical carcinogen, is bioactivated by cytochrome P450 (CYP) enzymes present in the liver, resulting in DNA adducts that form through an alkylation mechanism. DEN-induced liver cancer presents a gene expression profile similar to human HCC [40].

In the DEN-treated mouse model, liver tumors began to develop at age 30 weeks. R-Tf-D-LP4 treatment began at week 32 (Figure 3*A*). Mice were treated i.v. twice a week with HBSS alone or containing R-Tf-D-LP4 peptide at 10, 14, or 18 mg/kg from weeks 32 to 43 (Figure 3*A*). MRI showed that livers in untreated mice were big and occupied large abdominal volumes, while the livers of R-Tf-D-LP4–treated mice (18 mg/kg) were like those of DEN-untreated mice (Figure 3*B*).

All mice were sacrificed at week 43, and their livers were excised, photographed (Figure 3*C*), and weighed (Figure 3*D*). In control DEN-treated mice, numerous tumors of different sizes, occupying most of the liver area, were visible. These increased liver weight by about three-fold relative to the livers of mice not treated with DEN (Figure 3*D*). In livers from R-Tf-D-LP4 (18 mg/kg) DEN-treated mice, no tumors were visible, and liver weights were as those from mice not treated with DEN (Figure 3, *B-E*).

To analyze various tumor parameters, half of each liver was fixed and paraffin embedded, and sections were analyzed by H&E and IHC staining. The second half of each liver was frozen for further immunoblot analysis. H&E-stained liver sections (Figure 3, *E* and *F*) demonstrated large cancer nodules that were decreased in size and number in livers from R-Tf-D-LP4 and DEN-treated mice as function of peptide concentration; livers from mice treated with 18 mg/kg peptide displayed mostly normal liver parenchyma morphology (Figure 3*F*). Both the numbers and sizes of the tumor nodules were highly reduced as a function of R-Tf-D-LP4 concentration, approaching zero in mice treated with 18 mg/kg peptide (Figure 3, *G* and *H*).

Next, the DEN-induced HCC mice were treated with the peptide at week 37 post-DEN treatment (Figure 4*A*), when tumors were visible (Figure 4*B*). Mice were sacrificed at week 43, and their livers were excised, photographed (Figure 4, *C* and *D*), and weighed (Figure 4*E*). The livers from DEN-treated mice showed numerous tumors of different sizes (Figure 4*C*). In contrast, in livers from R-Tf-D-LP4 and DEN-treated mice, small tumors were visible in some livers, while others were tumor-free (Figure 4*D*). The decreases in both liver weight and the number of tumor nodules in the livers of mice treated with the peptide are shown (Figure 4, *E* and *F*).

Peptide Treatment Reprograms Cancer Cell Metabolism and Inhibits Cell Proliferation

R-Tf-D-LP4 peptide treatment of DEN-treated mice inhibited cell proliferation, as reflected in decreased levels of cell proliferation factor Ki-67 (Figure 5, *A* and *B*). Levels of positively Ki-67–stained nuclei were decreased by about 70% in livers of peptide (18 mg/kg)-treated mice (Figure 5*B*).

During malignant transformation, cancer metabolism is reprogramed. This involves increased expression levels of glucose transporters (Glut) and glycolytic enzymes [41]. Livers from peptide-treated DEN-exposed mice showed dramatically decreased expression levels of Glut-1, HK-II, GAPDH, and LDHA as compared to untreated mice (Figure 5*C*). Expression levels of the mitochondrial gatekeeper VDAC1, of the Kreb's cycle enzyme citrate synthase, and of ATP synthase 5a were also highly reduced in the livers of peptide-treated DEN-exposed mice (Figure 5*D*), consistent with alterations in oxidative phosphorylation (OXPHOS). Quantitative analysis of the IHC stained sections revealed a decrease by 90% of the staining intensity the peptide-treated livers relative to their levels in untreated livers Figure 5*E*).

The R-Tf-D-LP4 Peptide Induces Apoptosis and Overexpression of Proapoptotic Proteins

R-Tf-D-LP4 cell penetration is mediated by TfR, and as expected for cancer cells [36], the expression level of TfR was higher in livers from DEN-treated mice than in livers of mice not treated with DEN (Figure 6*A*). Also as expected, the peptide induced cell death, reflected in the presence of apoptotic cells *in situ*, as revealed by the presence of TUNEL-positive cells in R-Tf-D-LP4 and DEN-treated mice, with staining co-localizing with PI nuclear staining (Figure 6*B*).

Liver sections immunostained for the apoptosis-associated proteins Cyto *c* and AIF revealed increases in their expression levels in tumors from R-Tf-D-LP4 and DEN-treated mice (Figure 6*C*). Similarly, immunoblot analysis confirms these results and showed that expression levels of caspase-3 and caspase-8 were also increased three to six-fold (Figure 6, *D* and *E*). The results indicate that, as with cells in culture (Figures 1, *F* and *G*; 2, *E* and *F*), systemic administration of the peptides to DEN-exposed mice induced apoptotic cell death.

The VDAC1-Based Peptide R-Tf-D-LP4 Attenuates Tumor Microenvironment Activity

Liver cancer progression, like that of any other cancer, is associated with cancer microenvironment activity, such as inflammation, fibrosis, and angiogenesis [42]. Thus, the effects of R-Tf-D-LP4 on the tumor microenvironment in the DEN-treated mice were analyzed (Figure 7). Sirius red staining of collagen and intermediate filaments is

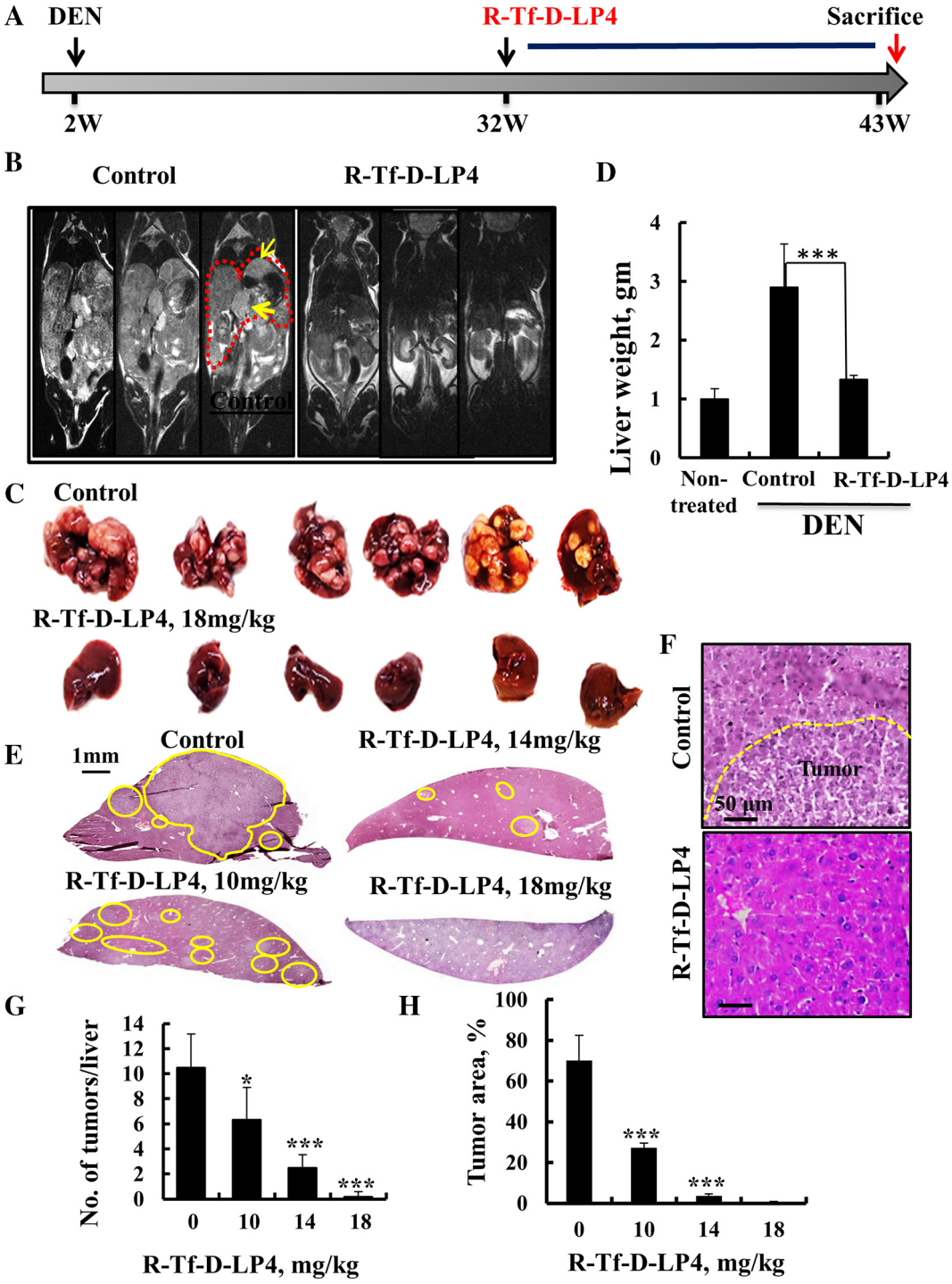

Figure 3. VDAC1-based peptide R-Tf-D-LP4 inhibits tumor growth in a DEN-induced mouse liver cancer model. (A) A schematic presentation of DEN-induced liver cancer development and treatment schedule. (B) MRI of the abdomens of 42-week-old mice treated i.v. with HBSS or R-Tf-D-LP4 (18 mg/kg, $n = 30$) for 10 weeks as described in Materials and Methods. (C, D) Dissected (C) and weighed (D) livers from DEN-treated, peptide-untreated, and R-Tf-D-LP4–treated DEN-mice. (E) H&E staining of liver sections from untreated and R-Tf-D-LP4–treated mice [0, 10, 14 mg/kg ($n = 8$) and 18 mg/kg, $n = 30$]. (F) A higher magnification of H&E staining of liver sections from untreated (with the tumor indicated) and R-Tf-D-LP4–treated mice (18 mg/kg) is shown. The numbers of tumors per liver (G) and tumor areas (H) were measured with a Pannoramic MIDI, 3DHISTECH microscope (Pannoramic viewer, 3DHISTECH). (*$P \leq .05$, ***$P \leq .001$).

associated with fibrosis/ cirrhosis in normal liver tissue and tumor-associated stromal activity [43]. In mice not treated with peptide, collagen fibers appeared in liver parenchyma and tumor tissue, whereas in R-Tf-D-LP4 and DEN-treated mice, collagen staining was highly decreased and was mostly observed around portal triads, as in normal liver tissue (Figure 7*A*).

α-SMA, a marker of myofibroblasts, is associated with pathological liver stellate cells activation into myofibroblasts-like cells [44], liver cirrhosis, cancer, and a poor prognosis [42,44]. α-SMA expression was observed in livers from untreated mice but not in R-Tf-D-LP4 and DEN-treated mice (Figure 7*B*), suggesting reduced fibrotic activity associated with reduced cancer stromal

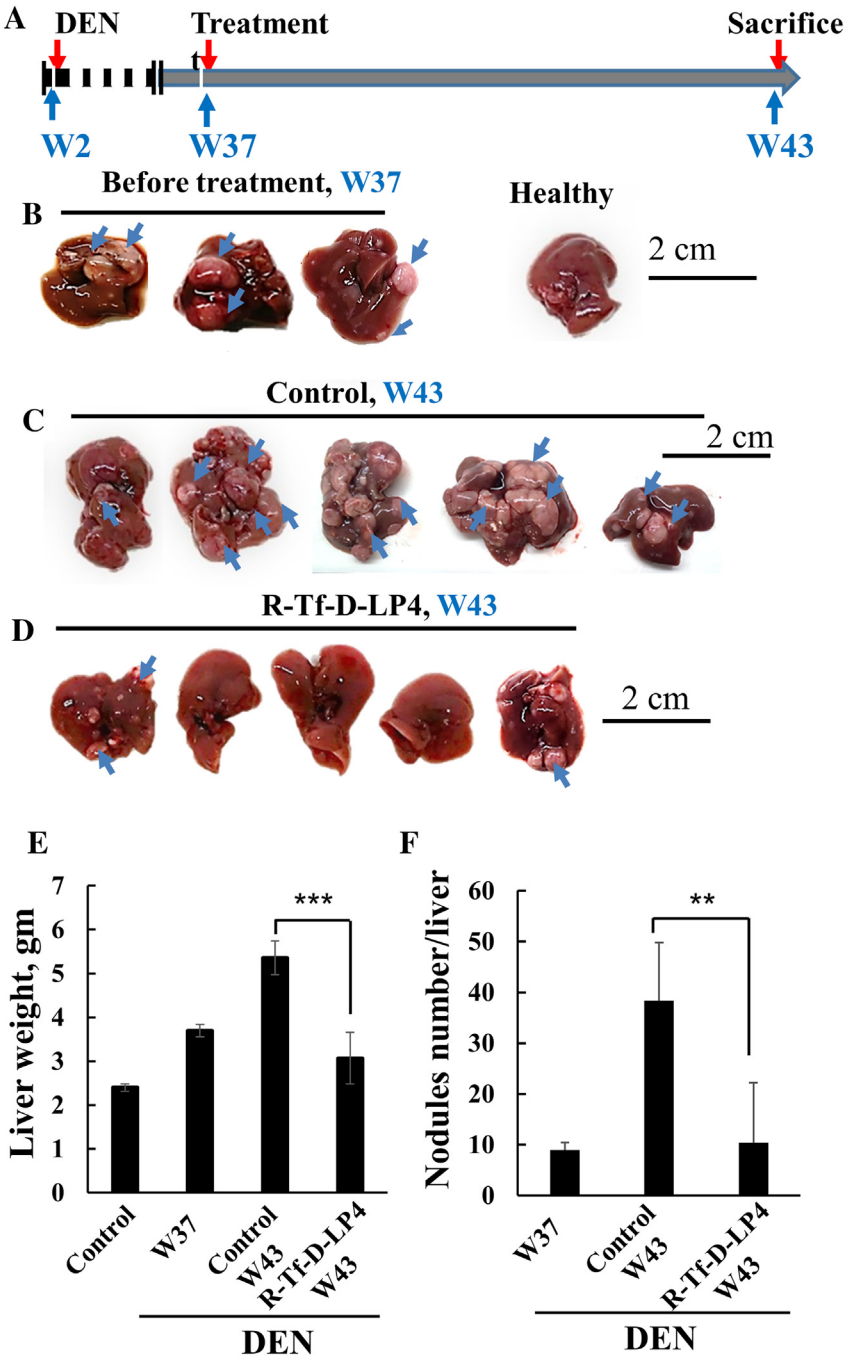

Figure 4. VDAC1-based peptide R-Tf-D-LP4 inhibits tumor growth in a DEN-induced mouse liver cancer model in a late disease stage. (A) A schematic presentation of DEN-induced liver cancer development and treatment schedule, weeks 37 to 43. (B) Dissected livers at week 37 from R-Tf-D-LP4–untreated DEN-treated mice. (C) Dissected livers at week 43 from R-Tf-D-LP4–untreated DEN-treated mice. (D) Dissected livers at week 43 from R-Tf-D-LP4 (18 mg/kg)–treated DEN-treated mice. (E) The weight of livers from DEN-untreated (control) and DEN-treated mice treated with R-Tf-D-LP4 (18 mg/kg) and untreated. (F) The amount of tumor nodules in livers from DEN-treated mice untreated and R-Tf-D-LP4 treated (18 mg/kg) (**$P \leq .01$, ***$P \leq .001$).

activity and cirrhosis. Moreover, the level of macrophage marker F4/80, associated with inflammation, fibrotic stimulation, and tumorigenicity, was decreased in peptide-treated mice (Figure 7*C*). In addition, the expression levels of B220+ and CD4+ cells were reduced by 46% and 33%, respectively, in the livers of peptide-treated mice. In contrast, T-cell markers, such as CD3+, CD8+, and FOXP3+ cells, were similarly expressed in livers from untreated and R-Tf-D-LP4–treated DEN-exposed mice (Figures 7, *D* and *E*).

Finally, H&E staining of liver sections from DEN-treated mice showed the pathology associated with steatosis, hepatocyte ballooning morphology, and inflammation. In contrast, livers from R-Tf-D-LP4 and DEN-treated mice showed no such pathology and instead resembled the livers from healthy mice not exposed to DEN (Figure 7*F*).

HFD-32–Induced Hepatocellular carcinoma (HCC)

The effects of the R-Tf-D-LP4 peptide on the pathology associated with steatosis in the DEN-exposed mice led us to test the effect of the

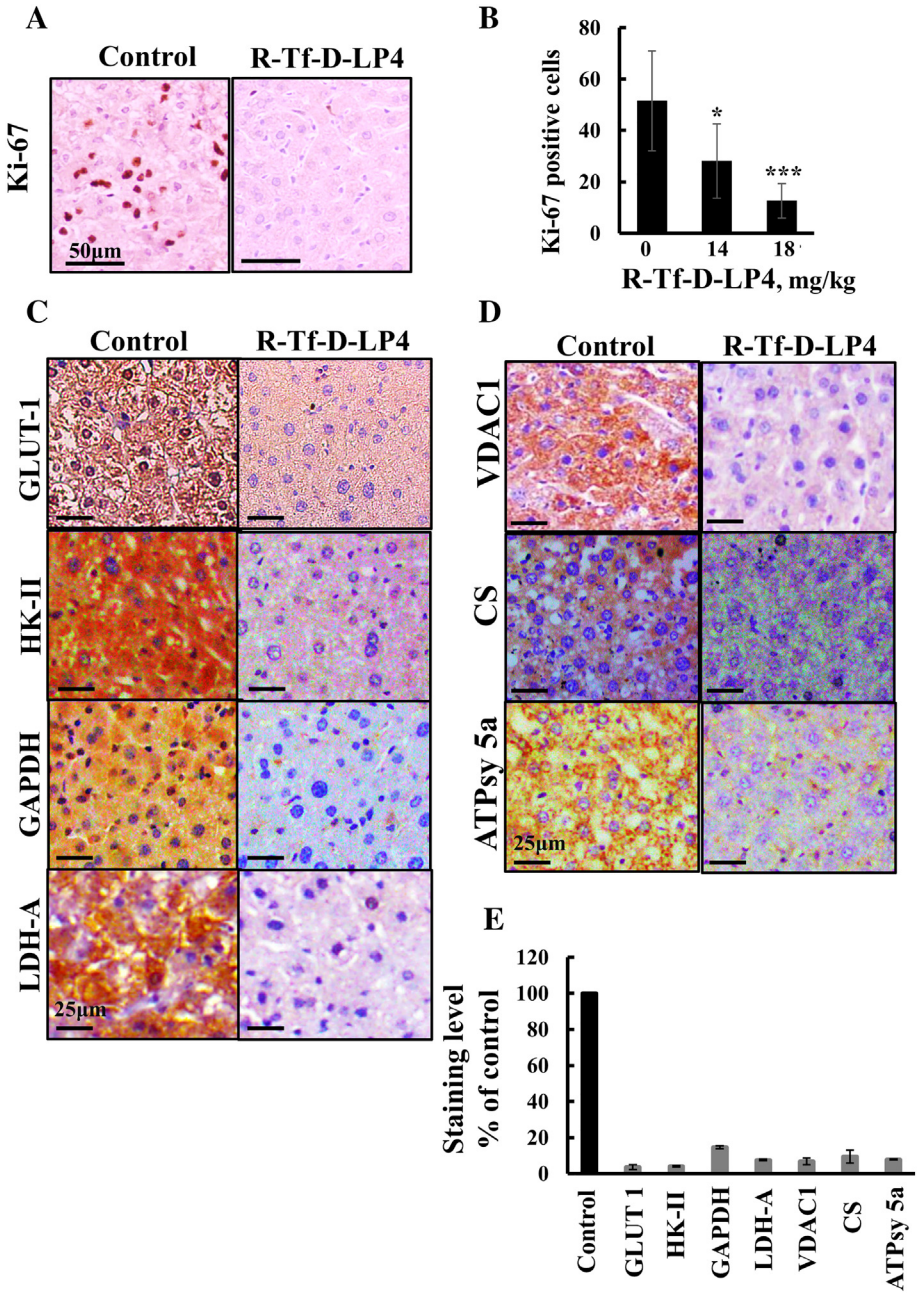

Figure 5. R-Tf-D-LP4 treatment of DEN-induced tumors reduces expression of metabolism-related enzymes and the proliferation marker Ki-67. (A) Representative liver sections from untreated and R-Tf-D-LP4–treated mice (18 mg/kg) stained with anti–Ki-67 antibodies and hematoxylin. (B) Quantitative analysis of Ki-67–positive cells (*$P \leq .05$, ***$P \leq .001$). Representative liver sections from untreated and R-Tf-D-LP4–treated mice were IHC stained for Glut-1, HK-II, GAPDH, and LDHA (C) and for VDAC1, citrate synthase, and ATP synthase 5a (D) using appropriate antibodies. Sections were also hematoxylin stained and visualized by microscopy (Leica DM2500). (E) Quantitative analysis of IHC-stained sections revealing intensity levels was carried out on panoramic scanner-generated images using HistoQuant software as described in Materials and Methods.

peptide on nonalcoholic steatohepatitis (NASH)–induced HCC development in the HFD-32, STAM mouse model. This model mimics metabolically induced HCC, a form of the disease that develops in nonalcoholic fatty liver disease/diabetic populations [57]. NASH-HCC was induced by a single s.c. low-dose (200 µg/mouse) injection of STZ into 2-day-old mice. From the end of week 4, the mice were fed with HFD-32, leading to the development of steatosis, followed by NASH and HCC (Figure 8*A*).

HFD-32 STAM mice were treated i.v. from 16 to 22 weeks with HBSS (peptide untreated) or with R-Tf-D-LP4 peptide (18 mg/kg). Mice were then sacrificed, and their livers were excised (Figure 8*B*), fixed, and analyzed by H&E staining (Figure 8*C*). Both the number of tumor nodules per liver (Figure 8*D*) and the tumor area (Figure 8*E*) were greatly decreased, with no tumors being found in the livers of the R-Tf-D-LP4–treated mice. Peptide treatment also dramatically reduced steatosis and inflammation (Figure 8*F*).

R-Tf-D-LP4 Inhibits HepG2-Derived Xenograft Tumor Growth

Finally, we tested the effects of the R-Tf-D-LP4 in a HepG2 xenograft mouse model (Figure 9). Athymic nude mice were injected

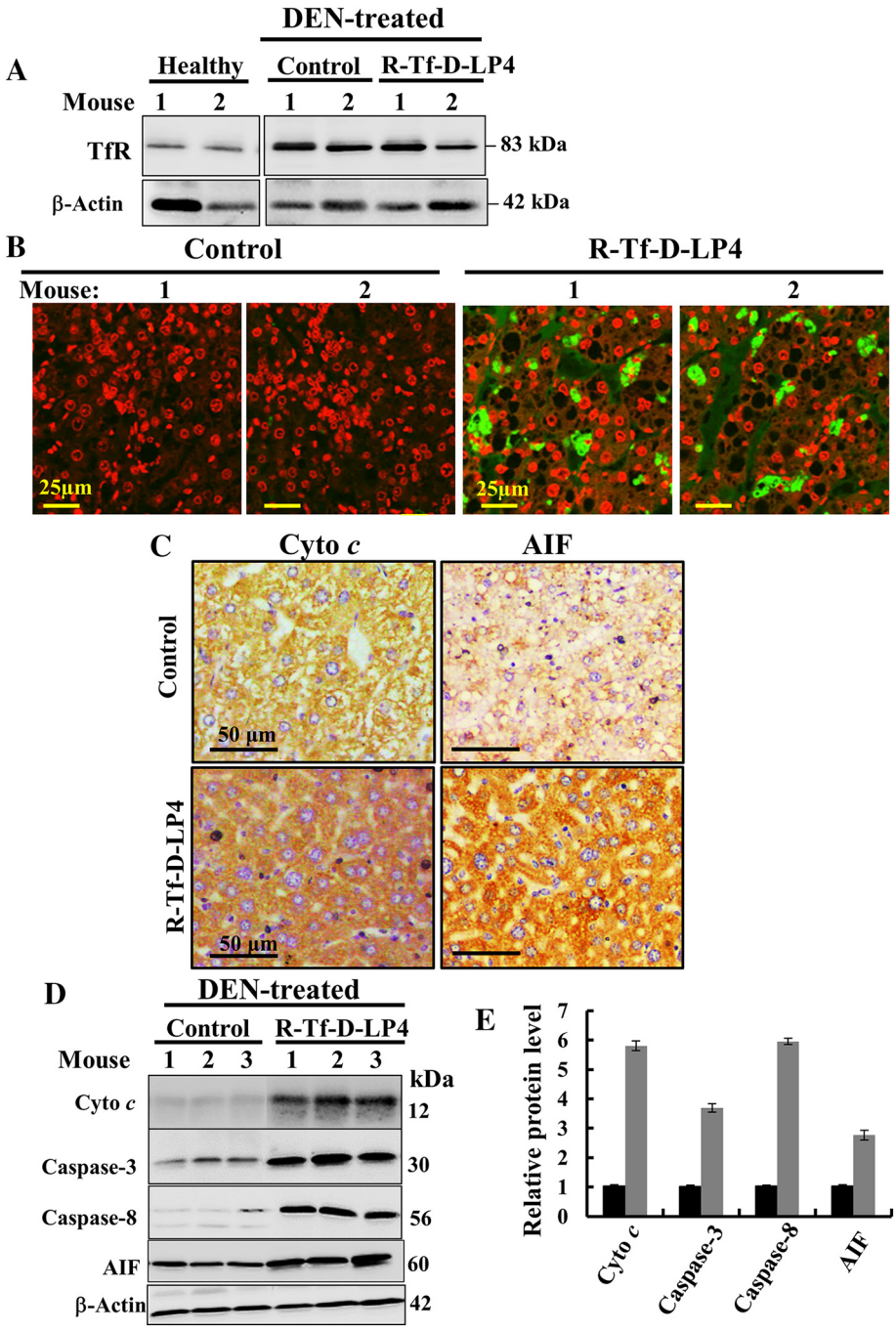

Figure 6. R-Tf-D-LP4 treatment of DEN-exposed mice induces apoptosis and modifies the expression of apoptosis-related proteins. (A) Immunoblot of TfR expression in DEN-untreated and DEN-induced liver tumors in untreated and R-Tf-D-LP4–treated mice analyzed by specific antibodies. β-Actin immunostaining is presented as a loading control. (B) TUNEL staining of liver sections from untreated and R-Tf-D-LP4–treated DEN-treated mice. Red and green colors indicate PI nuclear and TUNEL staining, respectively. (C) IHC of representative liver sections from untreated and R-Tf-D-LP4–treated mice stained with anti–Cyto *c* and anti-AIF antibodies. (D) Immunoblotting of liver lysates obtained from untreated and R-Tf-D-LP4–treated mice using anti–Cyto *c*, anti-AIF, anti–caspase-3, and anti–caspase-8 antibodies. (E) Quantitative analysis of the immunoblots as shown in (D) ($n = 3$). DEN-treated mice (black bars); DEN-treated mice and treated with the peptide (18 mg/kg) (gray bars).

s.c. with HepG2 hepatocellular cells. Following tumor formation (75-100 mm^3), the mice were split into two tumor volume-matched groups and treated intratumorally with HBSS (control) or with R-Tf-D-LP4 (final concentration of 40 μM) three times a week. In the peptide-untreated mice, tumor volume grew exponentially (Figure 9*A*), while the average tumor volume and weight in R-Tf-D-LP4–treated mice were about 30% to 35% of those of the control tumors (Figure 9, *B* and *C*).

Discussion

HCC is one of the most prevalent malignant diseases worldwide and is listed third in terms of cancer-related mortality. The high genetic

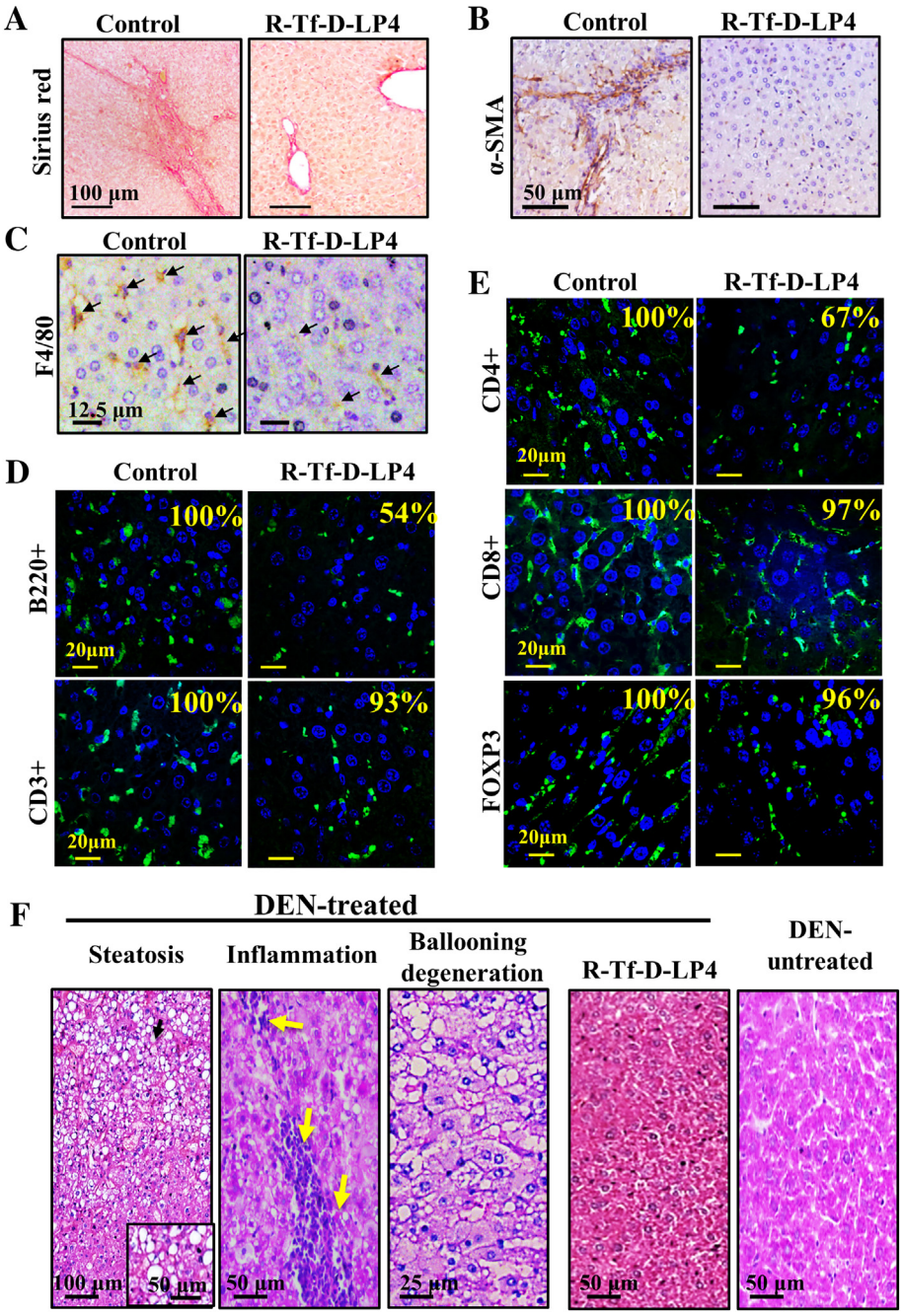

Figure 7. R-Tf-D-LP4 treatment of DEN-induced HCC eliminates hepatosteatotic pathology, inflammation, and fibrosis. (A-E) Representative liver sections from DEN-treated, R-Tf-D-LP4–untreated, or R-Tf-D-LP4–treated mice stained with Sirius red (A) or anti–α-SMA (B) or anti-F4/80 antibodies (C) showing macrophage infiltration. IF staining for CD3+ and B220 (D), CD4+, CD8+, or FOXP3 (E). The relative staining intensity (%) is presented in each image. The results are from several images from two mice for each antibody staining. (F) Representative liver sections, H&E stained, demonstrate hepatosteatosis pathology in DEN-induced liver tumors that were absent in R-Tf-D-LP4–treated mice.

and epigenetic heterogeneity of HCC tumors decreases the effectivity of a broad spectrum of treatment options [45]. Indeed, treatment of HCC remains challenging and requires new targets and novel therapeutic approaches that can also target fibrotic and inflammatory processes, as seen in liver parenchyma. Here, using various HCC cell lines *in vitro* and chemically induced, metabolically induced and xenograft HCC mouse models, we demonstrated the potential of the cell-penetrating VDAC1-based Tf-D-LP4 peptide as an innovative and effective treatment for HCC and associated pathologies. Tf-D-LP4 causes multiple effects, including perturbing cell energy homeostasis, inhibiting tumor growth, inducing cancer cell apoptosis, and attenuating processes associated with the liver cancer microenvironment, as well as steatosis, inflammation, and fibrosis.

The multiple effects of the peptide in DEN-treated mice and the findings that the peptide (18 mg/kg) intravenously administered three times per week for approximately 3 months had no effects on weight, physical activity, internal organ weight, or tissue morphology argue for the peptide as a promising anticancer agent.

VDAC1 is considered as a hub protein, with its interactome including proteins involved in metabolism, apoptosis, signal

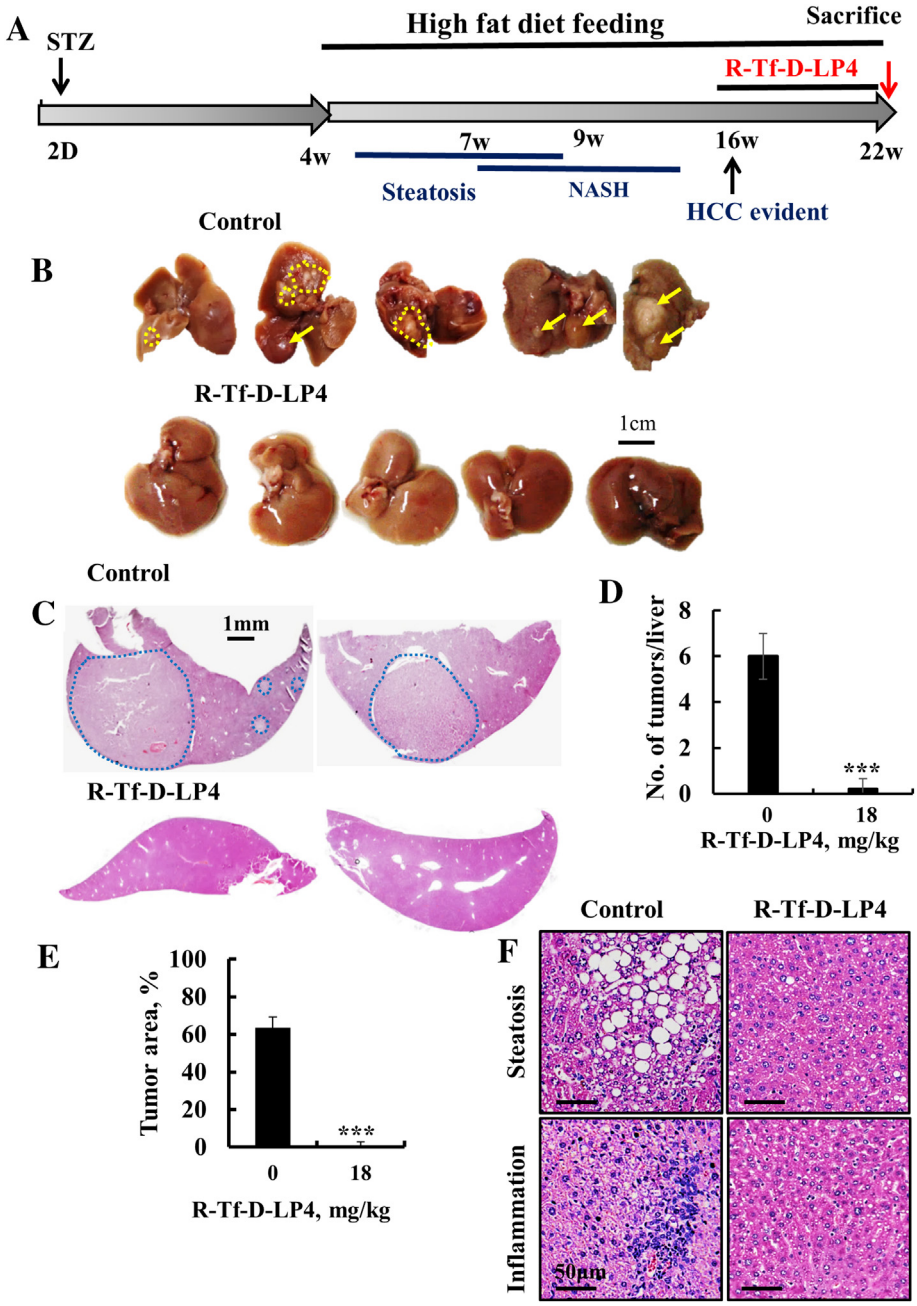

Figure 8. R-Tf-D-LP4 inhibits tumor growth in a metabolically (HFD-32) induced mouse hepatocellular carcinoma (NASH-HCC) model. (A) Schematic presentation of HFD-32–induced liver cancer development and treatment schedule. Mice were randomized into two groups. One group was treated i.v. with HBSS (control), and the second was treated with the R-Tf-D-LP4 (18 mg/kg) from week 16 until week 22, when the mice were sacrificed. (B) Dissected livers from untreated and R-Tf-D-LP4–treated mice (n = 10). (C) Liver sections from untreated and R-Tf-D-LP4–treated mice stained with H&E. Blue circles indicate the tumor. (D, E) The average number of tumors per liver and the relative tumor area were measured as in Figure 3*F*. Results show means ±SE (n = 5, ***$P \leq .001$). (F) Representative liver sections from untreated and R-Tf-D-LP4–treated mice stained with H&E showing steatosis and inflammation in peptide-untreated but not in R-Tf-D-LP4–treated mice.

transduction, antioxidation, and more [46]. The VDAC1-based peptide R-Tf-D-LP4 used here competes with VDAC1 for interactions with Bcl-2, Bcl-xL, and HK and consequently interrupts their antiapoptotic activities [19–21,26,37,47]. VDAC1-based peptides effectively induced cell death of cancer cell lines of different origin [35], including liver-derived cell lines, as shown here. The peptide perturbed cell energy status, as reflected by HK detachment; decreased cellular ATP levels; and induced Cyto *c* release and apoptosis despite the mutagenic diversity of the liver cancer cell lines tested (Figures 1, 2).

Overexpressed VDAC1 (Figure 1*A*) presents anchoring sites for overexpressed HK. VDAC1-bound HK not only lies at the apex of the glycolytic pathway but also protects against mitochondria-mediated cell death and decreases ROS production [14]. The disruption of VDAC1-HK interactions by the peptide presented here (Figure 2, *A* and *B*) and in other works [27,35] provides a strategy for interfering with cancer cell growth and activating cytochrome *c* release (Figure 2*D*) and apoptosis (Figure 1*D*; 2, *E* and *F*) [11,48]. The VDAC1-based peptide R-Tf-D-LP4 not only interacted with

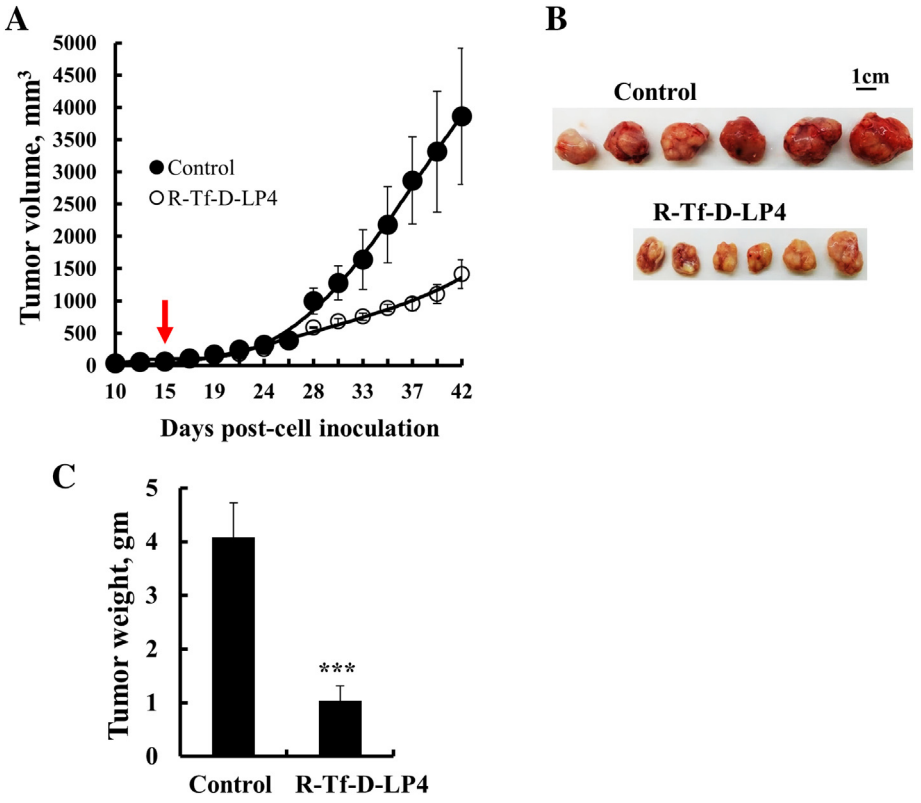

Figure 9. R-Tf-D-LP4 **i**nhibits tumor growth in a HepG2 xenograft mouse model. (A) HepG2 cells were inoculated into athymic nude mice as described in Materials and Methods. When the tumor volume was 75 to 100 mm^3, the mice were subdivided into two matched groups (five mice/group) and intratumorally injected every 2 days with HBSS (●, control) or R-Tf-D-LP4 (O, 40 μM). The calculated average tumor volumes are presented as mean ± SE ($n = 5$). Dissected tumors (B) and their weights (C). Results show means ± SE ($n = 11$) (*$P \leq .05$).

and detached HK from its binding site on VDAC1 (Figure 2, *A* and *B*) but also affected overall cellular bioenergetics by decreasing cellular ATP levels (Figure 2*C*) [21,26].

In the DEN-induced HCC, mice treated intravenously with R-Tf-D-LP4 revealed tumor growth inhibited up to complete elimination (Figure 3, *C-H*). The beginning of DEN-induced HCC after R-Tf-D-LP4 treatment at a late stage of disease (week 37) also showed promising results, with tumors being eliminated or the numbers and sizes of tumor nodules being reduced (Figure 4). Tumor growth was also inhibited in two other HCC models. In metabolically induced liver cancer in mice caused by STZ (reducing insulin production) and HFD-32, the peptide prevented tumor development (Figure 8), suggesting regulation of metabolic activity by R-Tf-D-LP4. Similarly, the peptide decreased tumor growth in a HepG2 cell xenograft mouse model (Figure 9). The dramatic effects of the peptide on tumor growth may result from its multiple effects disrupting tumor cell energy, inducing apoptosis, and altering the microenvironment.

Perturbing cell energy in R-Tf-D-LP4–treated mice was reflected in the marked decreases in the levels of the glycolytic enzymes HK-I, HK-II, GAPDH, and LDHA and Kreb's cycle enzymes (citrate synthase), and OXPHOS enzymes (ATP synthase 5a) (Figure 5, *C* and *D*). This is in line with studies suggesting that cancer cells use both glycolysis and OXPHOS and implies that the residual tumors from peptide-treated mice present reprogramed metabolism. The decreased metabolism also reflected decreased expression of the proliferative marker Ki-67 in livers from R-Tf-D-LP4–treated mice (Figure 5, *A* and *B*). In the residual tumors from the peptide-treated mice, massive apoptosis and elevated expression of proapoptotic proteins were also observed (Figure 6, *B* and *D*). Moreover, mice treated with R-Tf-D-LP4 (18 mg/kg) displayed decreased liver pathology in terms of steatohepatitis, inflammation, and fibrosis (Figure 7*F*). These effects of the peptide on tumor growth can be attributed to its action not only on two major cancer hallmarks, namely, the cancer cell energy status and induction of apoptotic cell death, but also on the tumor microenvironment.

Peptide treatment also led to diminished activation of liver stellate cells and their differentiation/activation into myofibroblasts-like cells (Figure 7*B*). This reduced inflammatory activity, as reflected in decreased macrophage numbers (Figure 7*C*) and a humoral response by the reduced number of B and CD4+ cells in the liver tissue of R-Tf-D-LP4–treated mice (Figure 7, *D* and *E*). Along with this, the number of CD3+, CD8+, and FOXP3+ (Tregs) T cells was similar in mice untreated and treated with the peptide (Figure 7, *D* and *E*).

Altogether, these results showed that peptide treatment not only reduced tumor burden but also attenuated the tumor microenvironment activity associated with noncancerous cells in the liver tissue, as demonstrated by peptide elimination of steatohepatitis features in DEN-treated mice. In addition, peptide treatment of DEN-induced HCC also decreased pathology-associated metabolic process, as liver fat accumulation, thereby preventing hepatocyte cells damage, inflammation, and fibrosis (Figure 7*F*). Similarly, in HFD-32-induced HCC, the peptide reduced steatosis and inflammation (Figure 8*F*). These multiple effects of the peptide involving alterations in the expression of proteins associated with metabolism and apoptosis affect the link between metabolism regulation and microenvironment activity.

To conclude, the role of tumorigenic metabolic rewiring in supporting cancer proliferation is well established, as are strategies developed by cancer cells for evading apoptosis, allowing them to overcome apoptotic cell death and display chemotherapy resistance. VDAC1 not only regulates metabolism but is also an apoptotic checkpoint in stress and pathological conditions. Considering the poor prognosis of liver cancer patients, the results presented here point to a VDAC1-based peptide as a potential new treatment for liver cancer. The effects of the peptide on cell energy and metabolism status, apoptosis induction, and microenvironment reorganization not only relieves cancer cell burden but also diminishes reasons for cancer development, as demonstrated in the HFD-32-NASH-HCC (STAM) model. Such a peptide treatment could replace several types of drugs, acting as a chemotherapy drug inducing apoptosis or inhibiting proliferation, cell metabolism or reducing tumor microenvironment activity.

Disclosure of Potential Conflicts of Interest

The authors declare no competing financial interests.

Acknowledgements

This research was supported by a grant from the Israel Science Foundation (307/13) and from Ezra and Yafa Yeruham and Sima and Philip Needleman research funds.

References

[1] Ferlay J, Soerjomataram I, Dikshit R, Eser S, Mathers C, Rebelo M, Parkin DM, Forman D, and Bray F (2015). Cancer incidence and mortality worldwide: sources, methods and major patterns in GLOBOCAN 2012. *Int J Cancer* **136**, E359-86.

[2] Wild CP and Gong YY (2010). Mycotoxins and human disease: a largely ignored global health issue. *Carcinogenesis* **31**, 71–82.

[3] Graziadei I, Zoller H, Fickert P, Schneeberger S, Finkenstedt A, Peck-Radosavljevic M, Muller H, Kohl C, Sperner-Unterweger B, and Eschertzhuber S, et al (2016). Indications for liver transplantation in adults : recommendations of the Austrian Society for Gastroenterology and Hepatology (OGGH) in cooperation with the Austrian Society for Transplantation, Transfusion and Genetics (ATX). *Wien Klin Wochenschr* **128**, 679–690.

[4] Shoshan-Barmatz V, Krelin Y, Shteinfer-Kuzmine A, and Arif T (2017). Voltage-dependent anion channel 1 as an emerging drug target for novel anti-cancer therapeutics. *Front Oncol* **7**, 154.

[5] Shoshan-Barmatz V, De Pinto V, Zweckstetter M, Raviv Z, Keinan N, and Arbel N (2010). VDAC, a multi-functional mitochondrial protein regulating cell life and death. *Mol Aspects Med* **31**, 227–285.

[6] Shoshan-Barmatz V and Mizrachi D (2012). VDAC1: from structure to cancer therapy. *Front Oncol* **2**, 164.

[7] Tsujimoto Y and Shimizu S (2002). The voltage-dependent anion channel: an essential player in apoptosis. *Biochimie* **84**, 187–193.

[8] Shoshan-Barmatz V, Israelson A, Brdiczka D, and Sheu SS (2006). The voltage-dependent anion channel (VDAC): function in intracellular signalling, cell life and cell death. *Curr Pharm Des* **12**, 2249–2270.

[9] Shoshan-Barmatz V, Mizrachi D, and Keinan N (2013). Oligomerization of the mitochondrial protein VDAC1: from structure to function and cancer therapy. *Prog Mol Biol Transl Sci* **117**, 303–334.

[10] Arif T, Vasilkovsky L, Refaely Y, Konson A, and Shoshan-Barmatz V (2014). Silencing VDAC1 expression by siRNA inhibits cancer cell proliferation and tumor growth in vivo. *Mol Ther Nucleic Acids* **3**e159.

[11] Shoshan-Barmatz V, Ben-Hail D, Admoni L, Krelin Y, and Tripathi SS (2015). The mitochondrial voltage-dependent anion channel 1 in tumor cells. *Biochim Biophys Acta* **1848**, 2547–2575.

[12] Shoshan-Barmatz V and Golan M (2012). Mitochondrial VDAC1: function in cell life and death and a target for cancer therapy. *Curr Med Chem* **19**, 714–735.

[13] Fulda S, Galluzzi L, and Kroemer G (2010). Targeting mitochondria for cancer therapy. *Nat Rev Drug Discov* **9**, 447–464.

[14] Hanahan D and Weinberg RA (2011). Hallmarks of cancer: the next generation. *Cell* **144**, 646–674.

[15] Shoshan-Barmatz V and Ben-Hail D (2012). VDAC, a multi-functional mitochondrial protein as a pharmacological target. *Mitochondrion* **12**, 24–34.

[16] Zaid H, Abu-Hamad S, Israelson A, Nathan I, and Shoshan-Barmatz V (2005). The voltage-dependent anion channel-1 modulates apoptotic cell death. *Cell Death Differ* **12**, 751–760.

[17] Abu-Hamad S, Arbel N, Calo D, Arzoine L, Israelson A, Keinan N, Ben-Romano R, Friedman O, and Shoshan-Barmatz V (2009). The VDAC1 N-terminus is essential both for apoptosis and the protective effect of anti-apoptotic proteins. *J Cell Sci* **122**, 1906–1916.

[18] Arbel N, Ben-Hail D, and Shoshan-Barmatz V (2012). Mediation of of the anti-apoptotic activity of Bcl-xL upon interaction with VDAC1. *J Biol Chem* **287**, 23152–23161.

[19] Arbel N and Shoshan-Barmatz V (2010). Voltage-dependent anion channel 1-based peptides interact with Bcl-2 to prevent antiapoptotic activity. *J Biol Chem* **285**, 6053–6062.

[20] Abu-Hamad S, Zaid H, Israelson A, Nahon E, and Shoshan-Barmatz V (2008). Hexokinase-I protection against apoptotic cell death is mediated via interaction with the voltage-dependent anion channel-1: mapping the site of binding. *J Biol Chem* **283**, 13482–13490.

[21] Arzoine L, Zilberberg N, Ben-Romano R, and Shoshan-Barmatz V (2009). Voltage-dependent anion channel 1-based peptides interact with hexokinase to prevent its anti-apoptotic activity. *J Biol Chem* **284**, 3946–3955.

[22] Zaid H, Abu-Hamad S, Israelson A, Nathan I, and Shoshan-Barmatz V (2005). The voltage-dependent anion channel-1 modulates apoptotic cell death. *Cell Death Differ* **12**, 751–760.

[23] Azoulay-Zohar H, Israelson A, Abu-Hamad S, and Shoshan-Barmatz V (2004). In self-defence: hexokinase promotes voltage-dependent anion channel closure and prevents mitochondria-mediated apoptotic cell death. *Biochem J* **377**, 347–355.

[24] Kontos CK, Christodoulou MI, and Scorilas A (2014). Apoptosis-related BCL2-family members: key players in chemotherapy. *Anticancer Agents Med Chem* **14**, 353–374.

[25] Lincet H and Icard P (2015). How do glycolytic enzymes favour cancer cell proliferation by nonmetabolic functions? *Oncogene* **34**, 3751–3759.

[26] Prezma T, Shteinfer A, Admoni L, Raviv Z, Sela I, Levi I, and Shoshan-Barmatz V (2013). VDAC1-based peptides: novel pro-apoptotic agents and potential therapeutics for B-cell chronic lymphocytic leukemia. *Cell Death Dis* **4**e809.

[27] Shteinfer-Kuzmine A, Arif T, Krelin Y, Tripathi SS, Paul A, and Shoshan-Barmatz V (2017). Mitochondrial VDAC1-based peptides: attacking oncogenic properties in glioblastoma. *Oncotarget* **8**, 31329–31346.

[28] Daniels TR, Bernabeu E, Rodriguez JA, Patel S, Kozman M, Chiappetta DA, Holler E, Ljubimova JY, Helguera G, and Penichet ML (2012). The transferrin receptor and the targeted delivery of therapeutic agents against cancer. *Biochim Biophys Acta* **1820**, 291–317.

[29] Kawai D, Takaki A, Nakatsuka A, Wada J, Tamaki N, Yasunaka T, Koike K, Tsuzaki R, Matsumoto K, and Miyake Y, et al (2012). Hydrogen-rich water prevents progression of nonalcoholic steatohepatitis and accompanying hepatocarcinogenesis in mice. *Hepatology* **56**, 912–921.

[30] Park TJ, Kim JY, Oh SP, Kang SY, Kim BW, Wang HJ, Song KY, Kim HC, and Lim IK (2008). TIS21 negatively regulates hepatocarcinogenesis by disruption of cyclin B1-Forkhead box M1 regulation loop. *Hepatology* **47**, 1533–1543.

[31] Fischer AH, Jacobson KA, Rose J, and Zeller R (2008). Hematoxylin and eosin staining of tissue and cell sections. *CSH Protoc* **2008** [pdb prot4986].

[32] Zhang Y, Xu N, Xu J, Kong B, Copple B, Guo GL, and Wang L (2014). E2F1 is a novel fibrogenic gene that regulates cholestatic liver fibrosis through the Egr-1/SHP/EID1 network. *Hepatology* **60**, 919–930.

[33] Abu-Hamad S, Sivan S, and Shoshan-Barmatz V (2006). The expression level of the voltage-dependent anion channel controls life and death of the cell. *Proc Natl Acad Sci U S A* **103**, 5787–5792.

[34] Koren I, Raviv Z, and Shoshan-Barmatz V (2010). Downregulation of voltage-dependent anion channel-1 expression by RNA interference prevents cancer cell growth in vivo. *Cancer Biol Ther* **9**, 1046–1052.

[35] Shteinfer-Kuzmine A, Amsalem Z, Arif T, Zooravlov A, and Shoshan-Barmatz V (2018). Selective induction of cancer cell death by VDAC1-based peptides and their potential use in cancer therapy. *Mol Oncol* (in press).

[36] Herbison CE, Thorstensen K, Chua AC, Graham RM, Leedman P, Olynyk JK, and Trinder D (2009). The role of transferrin receptor 1 and 2 in transferrin-bound iron uptake in human hepatoma cells. *Am J Physiol Cell Physiol* **297**, C1567–1575.

[37] Abu-Hamad S, Arbel N, Calo D, Arzoine L, Israelson A, Keinan N, Ben-Romano R, Friedman O, and Shoshan-Barmatz V (2009). The VDAC1 N-

terminus is essential both for apoptosis and the protective effect of anti-apoptotic proteins. *J Cell Sci* **122**, 1906–1916.

[38] Pastorino JG, Shulga N, and Hoek JB (2002). Mitochondrial binding of hexokinase II inhibits Bax-induced cytochrome c release and apoptosis. *J Biol Chem* **277**, 7610–7618.

[39] Nederlof R, Eerbeek O, Hollmann MW, Southworth R, and Zuurbier CJ (2014). Targeting hexokinase II to mitochondria to modulate energy metabolism and reduce ischaemia-reperfusion injury in heart. *Br J Pharmacol* **171**, 2067–2079.

[40] Verna L, Whysner J, and Williams GM (1996). N-nitrosodiethylamine mechanistic data and risk assessment: bioactivation, DNA-adduct formation, mutagenicity, and tumor initiation. *Pharmacol Ther* **71**, 57–81.

[41] Koppenol WH, Bounds PL, and Dang CV (2011). Otto Warburg's contributions to current concepts of cancer metabolism. *Nat Rev Cancer* **11**, 325–337.

[42] Tahmasebi Birgani M and Carloni V (2017). Tumor microenvironment, a paradigm in hepatocellular carcinoma progression and therapy. *Int J Mol Sci* **18**.

[43] Kubo N, Araki K, Kuwano H, and Shirabe K (2016). Cancer-associated fibroblasts in hepatocellular carcinoma. *World J Gastroenterol* **22**, 6841–6850.

[44] Friedman SL (2008). Hepatic stellate cells: protean, multifunctional, and enigmatic cells of the liver. *Physiol Rev* **88**, 125–172.

[45] Ziogas IA and Tsoulfas G (2017). Evolving role of Sorafenib in the management of hepatocellular carcinoma. *World J Clin Oncol* **8**, 203–213.

[46] Shoshan-Barmatz V, Maldonado EN, and Krelin Y (2017). VDAC1 at the crossroads of cell metabolism, apoptosis and cell stress. *Cell Stress* **1**, 11–36.

[47] Arbel N, Ben-Hail D, and Shoshan-Barmatz V (2012). Mediation of the antiapoptotic activity of Bcl-xL protein upon interaction with VDAC1 protein. *J Biol Chem* **287**, 23152–23161.

[48] Krasnov GS, Dmitriev AA, Lakunina VA, Kirpiy AA, and Kudryavtseva AV (2013). Targeting VDAC-bound hexokinase II: a promising approach for concomitant anti-cancer therapy. *Expert Opin Ther Targets* **17**, 1221–1233.

[49] Ewald F, Norz D, Grottke A, Bach J, Herzberger C, Hofmann BT, Nashan B, and Jucker M (2015). Vertical targeting of AKT and mTOR as well as dual targeting of AKT and MEK signaling is synergistic in hepatocellular carcinoma. *J Cancer* **6**, 1195–1205.